

Observation of Body-Centered Cubic Gold Nanocluster**

Chao Liu, Tao Li, Gao Li, Katsuyuki Nobusada, Chenjie Zeng, Guangsheng Pang,
Nathaniel L. Rosi, and Rongchao Jin*

Abstract: The structure of nanoparticles plays a critical role in dictating their material properties. Gold is well known to adopt face-centered cubic (fcc) structure. Herein we report the first observation of a body-centered cubic (bcc) gold nanocluster composed of 38 gold atoms protected by 20 adamantanethiolate ligands and two sulfido atoms ($[Au_{38}S_2(SR)_{20}]$, where $R = C_{10}H_{15}$) as revealed by single-crystal X-ray crystallography. This bcc structure is in striking contrast with the fcc structure of bulk gold and conventional Au nanoparticles, as well as the bi-icosahedral structure of $[Au_{38}(SCH_2CH_2Ph)_{24}]$. The bcc nanocluster has a distinct HOMO–LUMO gap of ca. 1.5 eV, much larger than the gap (0.9 eV) of the bi-icosahedral $[Au_{38}(SCH_2CH_2Ph)_{24}]$. The unique structure of the bcc gold nanocluster may be promising in catalytic applications.

Determining the structure of nanoclusters, in particular the surface structure, is of major importance for understanding their catalytic properties.^[1] In recent research, atomically precise gold nanoclusters have emerged as a new frontier and significant progress has been made in both experimental^[2–14] and theoretical research.^[15–19] These nanoclusters are composed of specific numbers of gold atoms ranging from a dozen to hundreds and are also protected by specific numbers of ligands. The total structures (i.e. gold core and ligand arrangements) of nanoclusters can be solved by single-crystal X-ray crystallography.^[20–33] This new class of nanomaterial has several unique features^[34] compared to conventional gold nanoparticles: 1) the ultra-small size of nanoclusters induces strong quantum size effects, manifested in the disappearance of surface plasmon resonance and strong quantization of the electronic energy bands,^[20] 2) non-crystallographic structures (i.e. without translational symmetry in the metal core) are found to be prevalent in nanoclusters as opposed to the face-centered cubic (fcc) structure in bulk gold and relatively large nanoparticles (> 2 nm). Various types of ligands have been

explored in the syntheses of nanoclusters, including phosphine,^[21–24] thiolate,^[34] alkynyl,^[35–37] and mixed ligands.^[29–32] The ligand structure has been found to play an important role in controlling the kernel and surface structures of nanoclusters;^[28] for example, Zeng et al. obtained the fcc-structured $[Au_{36}(SPh-tBu)_{24}]$ nanocluster protected by unprecedented bridging thiolate -S(R)- together with the common -S(R)-Au-S(R)-Au-S(R)- dimeric staple motif.^[28] Recently, Wan et al. reported the alkynyl/phosphine-protected Au_{19} nanocluster structure featuring the $PhC \equiv C-Au-C \equiv C(Ph)-Au-C \equiv CPh$ motif^[37]—which resembles the -S(R)-Au-S(R)-Au-S(R)- dimeric staple motif.

Herein, we report the first observation of a body-centered cubic (bcc) structured gold nanocluster. This nanocluster contains 38 gold atoms and is protected by two sulfido (-S-) and twenty adamantanethiolate ligands (S-Adm). The observed bcc structure is in striking contrast to the fcc and other structures reported for gold nanoclusters.^[34]

The $[Au_{38}S_2(S-Adm)_{20}]$ nanocluster was synthesized by a size-focusing method^[38] and details are provided in the Experimental Section. It consists of two primary steps, 1) the synthesis of polydispersed crude nanoclusters with a controlled size range (5–13 kDa), and 2) size focusing of the polydispersed nanoclusters into a monodispersed product under thermal conditions (90 °C for ca. 24 h) in the presence of excess adamantanethiol. The final nanoclusters were crystallized by a vapor diffusion method.

The $[Au_{38}S_2(S-Adm)_{20}]$ crystal structure adopts a monoclinic space group, $P2_1/n$. The total structure is shown in Figure 1, with the 20 thiolate ligands distributed in C_{2v} symmetry and the two bare sulfur atoms bonded to the Au atoms in a tripodal fashion (Figure 2A, highlighted by the arrows). After removing the adamantane groups, the $Au_{38}S_{22}$ framework clearly shows C_{2v} symmetry (Figure 2A,B). Among the 38 gold atoms, eight of them are a relatively

[*] C. Liu, Dr. G. Li, C. Zeng, Prof. R. Jin
Department of Chemistry
Carnegie Mellon University
Pittsburgh, PA 15213 (USA)
E-mail: rongchao@andrew.cmu.edu


C. Liu, Prof. G. Pang
State Key Laboratory of Inorganic Synthesis and Preparative
Chemistry, Jilin University
2699 Qianjin Street, Changchun, Jilin 130012 (P. R. China)

T. Li, Prof. N. L. Rosi
Department of Chemistry, University of Pittsburgh
Pittsburgh, PA 15260 (USA)

Prof. K. Nobusada
Department of Theoretical and Computational Molecular Science
Institute for Molecular Science
Myodaiji, Okazaki, 444-8585 (Japan)

and
Elements Strategy Initiative for Catalysts and Batteries (ESICB)
Kyoto University, Katsura, Kyoto 615-8520 (Japan)

[**] R.J. acknowledges support by the Air Force Office of Scientific Research under AFOSR Award No. FA9550-15-1-9999 (FA9550-15-1-0154). K.N. acknowledges support by Grant in Aid (No. 25288012), MEXT, and by the MEXT program “Elements Strategy Initiative to Form Core Research Center” (since 2012). The computation was also partly performed at the Research Center for Computational Science, Okazaki (Japan). C.L. acknowledges the fellowship support by China Scholarship Council. S.P. acknowledges support by National Natural Science Foundation of China (21071058).

 Supporting information for this article is available on the WWW under <http://dx.doi.org/10.1002/anie.201502667>.

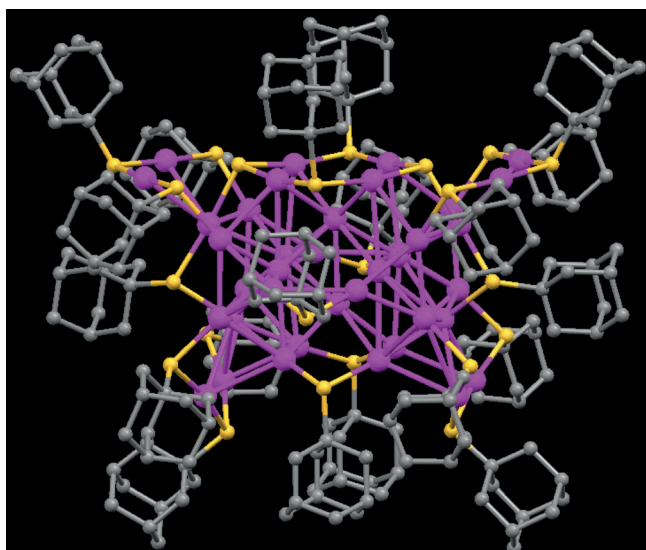


Figure 1. X-ray structure of $[\text{Au}_{38}\text{S}_2(\text{S-Adm})_{20}]$ (magenta Au, yellow S, gray C, all H atoms are omitted for clarity).

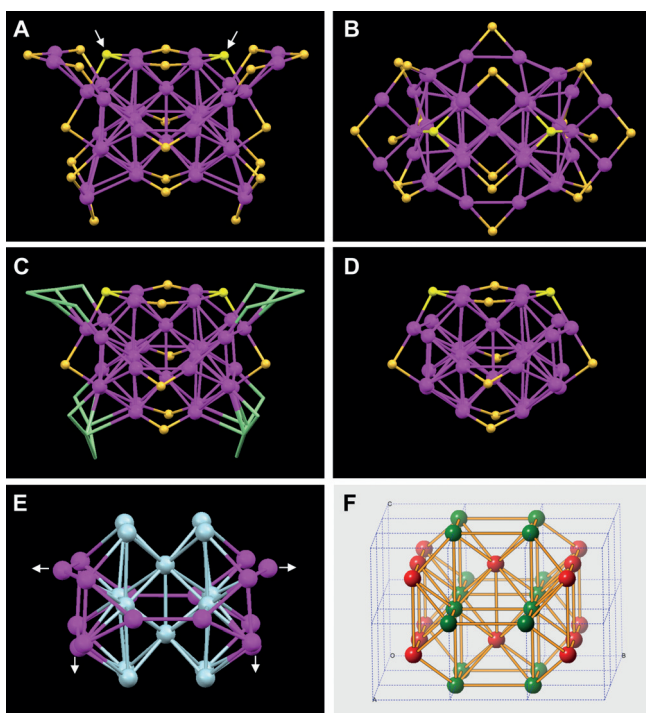


Figure 2. A,B) side and top views of the $\text{Au}_{38}\text{S}_{22}$ framework, arrows indicate the two bare S atoms. C) Assignment of four staple-like motifs (green), D) the $\text{Au}_{30}\text{S}_{10}$ inner unit, E) the bcc Au_{30} kernel (the slight distortions are indicated by the arrows), and F) the ideal bcc Au_{30} kernel carved out of a bcc array of 3 unit cells long \times 3 unit cells wide \times 2 unit cells high (yellow S, other colors are all for Au).

large Au–Au distance (3.0–3.3 Å) from the inner gold atoms and may be assigned as four –SR–Au–SR–Au–SR– dimeric staple motifs (Figure 2C, highlighted in green wireframes). Removing the four staple motifs gives rise to $\text{Au}_{30}\text{S}_{10}$ (Figure 2D), in which the Au_{30} unit indeed constitutes a bcc structure. To show clearly the bcc arrangement of Au_{30} , we remove the two tripodal S atoms and other eight S atoms, and

compare the resultant Au_{30} (Figure 2E) with the ideal bcc arrangement of 30 gold atoms in the bcc lattice (Figure 2F); the ideal Au_{30} bcc structure is enclosed in a $3 \times 3 \times 2$ multi-cell bcc lattice (Figure 2F) and comprises 14 centers of bcc and 16 vertices of bcc (Figure 2F, red and green, respectively). By comparing with the ideal 30-atom bcc structure, the central part of the experimental Au_{30} structure consists of two bcc cubes stacked vertically (comparing Figure 2E and 2F), forming an Au_{14} inner core, and the remaining 16 Au atoms further extend the inner core according to the bcc structural arrangement (comparing Figure 2E and 2F). Note that the bonding between the Au_{30} unit and the gold atoms in the dimeric staple motifs slightly pulls four gold atoms out of the ideal bcc positions (see arrows in Figure 2E).

The two sulfido atoms in the bcc- Au_{38} cluster should originate from adamantanethiol, which may undergo S–C bond cleavage^[39,40] under heating conditions during the size-focusing step. The structure of $[\text{Au}_{38}\text{S}_2(\text{S-Adm})_{20}]$ is unique in that it exhibits not only the bcc core but also many different types of facets, including triangular Au_3 , square Au_4 , trapezoidal Au_5 , and hexagonal Au_6 facets (Figure 3). To gain

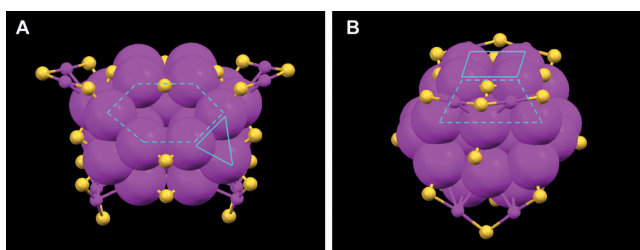


Figure 3. The gold facets on the $[\text{Au}_{38}\text{S}_2(\text{S-Adm})_{20}]$ nanocluster. A) triangular Au_3 and hexagonal Au_6 facets, B) square Au_4 and trapezoidal Au_5 facets. The structure in (B) is rotated by 90° with respect to (A). (magenta Au, yellow S).

further insight into the structure of $[\text{Au}_{38}\text{S}_2(\text{S-Adm})_{20}]$, we carried out density functional theory (DFT) calculations (see Supporting Information for details). The $[\text{Au}_{38}\text{S}_2(\text{S-Adm})_{20}]$ nanocluster was simplified as $[\text{Au}_{38}\text{S}_2(\text{SCH}_3)_{20}]$ by replacing the adamantane group with a methyl group. We first simulated the optical absorption spectrum of $[\text{Au}_{38}\text{S}_2(\text{SCH}_3)_{20}]$ for comparison with the experimental spectrum of $[\text{Au}_{38}\text{S}_2(\text{S-Adm})_{20}]$ which shows absorption peaks at 650 and 750 nm (Figure 4A). The theoretical spectrum is convoluted

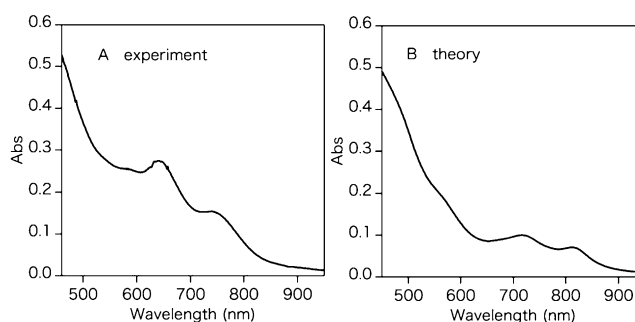


Figure 4. Optical absorption spectra of $[\text{Au}_{38}\text{S}_2(\text{S-Adm})_{20}]$ (experiment) and $[\text{Au}_{38}\text{S}_2(\text{SCH}_3)_{20}]$ (theory).

by the Lorentz function with appropriate width (Figure 4B). The DFT simulations reproduced the experimental spectral profile with the same double-peak feature (Figure 4B), albeit the theoretical peak wavelengths (715 and 810 nm) deviated from the experimental peak positions (650 and 750 nm). The simulated 715 nm peak (corresponding to experimental 650 nm) primarily arises from the HOMO to LUMO + 2 electronic transition, and the 810 nm peak (corresponding to experimental 750 nm) arises from HOMO to LUMO transition. Thus, the experimentally observed peak at 750 nm is due to a HOMO–LUMO transition, and by extrapolating the optical absorbance to zero the HOMO–LUMO gap is determined to be approximately 1.5 eV, which is much larger than the 0.9 eV energy gap of the bi-icosahedral 38-atom $[\text{Au}_{38}(\text{SC}_2\text{H}_4\text{Ph})_{24}]$ nanocluster,^[41] implying the gold-atom arrangement influences the energy gap and electronic properties.

The simulated HOMO of $[\text{Au}_{38}\text{S}_2(\text{SCH}_3)_{20}]$ is shown in Figure S1 in the Supporting Information. The HOMO distribution shows that the two bottom dimeric staples (see the geometric structure in Figure 2C) are merged into the Au_{30} bcc core structure, while the two top dimeric staples are not so involved in the core. Figure S1B shows the top view of HOMO of $[\text{Au}_{38}\text{S}_2(\text{SCH}_3)_{20}]$, indicating that each bare S atom serves as an anchor triply bridging the Au_{30} bcc core and might play an important role in stabilizing the new structural characteristic of this gold thiolate nanocluster with the bcc structure. Note that $[\text{Au}_{38}\text{S}_2(\text{S-Adm})_{20}]$ has a nominal 20 free valence electrons, the same as $[\text{Au}_{38}(\text{SC}_2\text{H}_4\text{Ph})_{24}]$.

The various types of facets (Figure 3) exhibited by this bcc- Au_{38} nanocluster are potentially of interest for future catalytic studies. The pocket-like surface structures can serve as catalytic sites for adsorbing and activating reactant molecules; for instance, Li et al. reported the reactant activation on the Au_3 pocket sites on $[\text{Au}_{25}(\text{SC}_2\text{H}_4\text{Ph})_{18}]$.^[42] The multi-atom, cavity-like sites on the surface of the bcc-structured $[\text{Au}_{38}\text{S}_2(\text{S-Adm})_{20}]$ are expected to be more effective in adsorbing reactant molecules owing to the multi-atom binding effect. These surface sites may also be explored in electrocatalytic CO_2 conversion to fuels since CO_2 was also activated by multi-atom sites.^[1]

In conclusion, the bcc structure of $[\text{Au}_{38}\text{S}_2(\text{S-Adm})_{20}]$ came as a surprise, as no bcc structure has been previously observed in gold nanoclusters or larger gold nanoparticles. Its occurrence is attributed to the adamantanethiol ligand. The adamantanethiol^[43] and other bulky ligands^[44–46] may be further explored in future work for size-controlled synthesis of $[\text{Au}_n(\text{SR})_m]$ nanoclusters. Overall, this work demonstrates that the specific atomic arrangement in the Au_{38} nanocluster can largely affect the HOMO–LUMO gap, electronic structure, and optical absorption. This new material may find promising applications (such as catalysis) in future research.

Experimental Section

$[\text{Au}_{38}\text{S}_2(\text{SR})_{20}]$: The $[\text{Au}_{38}\text{S}_2(\text{SR})_{20}]$ nanocluster (SR = adamantanethiolate) was synthesized following a size-focusing method^[14]. In a typical experiment, $\text{HAuCl}_4 \cdot 3\text{H}_2\text{O}$ (78.8 mg, 0.2 mmol) and tetraoctylammonium bromide (TOAB, 109.4 mg, 0.2 mmol) were mixed in

THF (15 mL) at room temperature, and stirred for 30 min. After that, adamantanethiol (134.4 mg, 0.8 mmol) was added and stirred vigorously until the solution turned colorless [that is, complete conversion of Au^{III} to Au^{I}]. Then, a freshly made NaBH_4 solution (76 mg, 2 mmol, dissolved in 5 mL cold Nanopure water) was added to the reaction mixture all at once. The solution immediately turned dark. After 10 min, the solution containing the crude product was evaporated to near dryness. The black product (containing nanoclusters) was washed with methanol for four times. The solid was then extracted with CH_2Cl_2 . The species insoluble in CH_2Cl_2 were discarded. The extracted nanocluster solution (in CH_2Cl_2) was evaporated to dryness, then extracted for a second time. Finally, the cluster solution was evaporated to dryness, and 50 mg solid was obtained. The as-obtained nanoclusters contained a mixture of different sizes which were converted into monodisperse nanoclusters following a size-focusing step. For the size-focusing step, the nanoclusters were mixed with excess adamantanethiol (252 mg, 1.5 mmol) and co-dissolved in toluene (2 mL). The solution was heated to 90 °C and maintained at this temperature for more than 24 h. The final product was washed with methanol for four times and then extracted with CH_2Cl_2 (repeated three times). The finally extracted CH_2Cl_2 solution contained quite pure $[\text{Au}_{38}\text{S}_2(\text{SR})_{20}]$ nanoclusters. The as-obtained $[\text{Au}_{38}\text{S}_2(\text{SR})_{20}]$ nanoclusters were crystallized by methanol vapor diffusion into a toluene solution of nanoclusters. Details of X-ray diffraction analysis and density functional theory calculations are provided in the Supporting Information.

Keywords: body-centered cubic · gold · nanoclusters · structure elucidation

How to cite: *Angew. Chem. Int. Ed.* **2015**, *54*, 9826–9829
Angew. Chem. **2015**, *127*, 9964–9967

- [1] G. Li, R. Jin, *Acc. Chem. Res.* **2013**, *46*, 1749–1758.
- [2] A. Das, C. Liu, H. Y. Byun, K. Nobusada, S. Zhao, N. L. Rosi, R. Jin, *Angew. Chem. Int. Ed.* **2015**, *54*, 3140–3144; *Angew. Chem.* **2015**, *127*, 3183–3187.
- [3] S. Chen, S. Wang, J. Zhong, Y. Song, J. Zhang, H. Sheng, Y. Pei, M. Zhu, *Angew. Chem. Int. Ed.* **2015**, *54*, 3145–3149; *Angew. Chem.* **2015**, *127*, 3188–3192.
- [4] N. K. Chaki, Y. Negishi, H. Tsunoyama, Y. Shichibu, T. Tsukuda, *J. Am. Chem. Soc.* **2008**, *130*, 8608–8610.
- [5] X. Yuan, B. Zhang, Z. Luo, Q. Yao, D. T. Leong, N. Yan, J. Xie, *Angew. Chem. Int. Ed.* **2014**, *53*, 4623–4627; *Angew. Chem.* **2014**, *126*, 4711–4715.
- [6] Y. Negishi, K. Munakata, W. Ohgake, K. Nobusada, *J. Phys. Chem. Lett.* **2012**, *3*, 2209–2214.
- [7] S. Knoppe, O. A. Wong, S. Malola, H. Häkkinen, T. Bürgi, T. Verbiest, C. J. Ackerson, *J. Am. Chem. Soc.* **2014**, *136*, 4129–4132.
- [8] X.-K. Wan, S.-F. Yuan, Z.-W. Lin, Q.-M. Wang, *Angew. Chem. Int. Ed.* **2014**, *53*, 2923–2926; *Angew. Chem.* **2014**, *126*, 2967–2970.
- [9] Y. Kamei, Y. Shichiba, K. Konishi, *Angew. Chem. Int. Ed.* **2011**, *50*, 7442–7445; *Angew. Chem.* **2011**, *123*, 7580–7583.
- [10] A. Ghosh, T. Udayabhaskararao, T. Pradeep, *J. Phys. Chem. Lett.* **2012**, *3*, 1997–2002.
- [11] Q. Yao, Y. Yu, X. Yuan, Y. Yu, J. Xie, J. Y. Lee, *Small* **2013**, *9*, 2696–2701.
- [12] H. Yao, *J. Phys. Chem. Lett.* **2012**, *3*, 1701–1706.
- [13] J. Zheng, C. Zhou, M. Yu, J. Liu, *Nanoscale* **2012**, *4*, 4073–4083.
- [14] H. Qian, Y. Zhu, R. Jin, *Proc. Natl. Acad. Sci. USA* **2012**, *109*, 696–700.
- [15] D.-E. Jiang, S. H. Overbury, S. Dai, *J. Am. Chem. Soc.* **2013**, *135*, 8786–8789.
- [16] S. Malola, L. Lehtovaara, S. Knoppe, K.-J. Hu, R. E. Palmer, T. Bürgi, H. Häkkinen, *J. Am. Chem. Soc.* **2012**, *134*, 19560–19563.

- [17] A. Tlahuice, I. L. Garzon, *Phys. Chem. Chem. Phys.* **2012**, *14*, 3737–3740.
- [18] Y. Pei, R. Pal, C. Liu, Y. Gao, Z. Zhang, X. C. Zeng, *J. Am. Chem. Soc.* **2012**, *134*, 3015–3024.
- [19] E. B. Guidez, V. Mäkinen, H. Häkkinen, C. M. Aikens, *J. Phys. Chem. C* **2012**, *116*, 20617–20624.
- [20] H. Qian, M. Zhu, Z. Wu, R. Jin, *Acc. Chem. Res.* **2012**, *45*, 1470–1479.
- [21] Y. Shichibu, M. Zhang, Y. Kamei, K. Konishi, *J. Am. Chem. Soc.* **2014**, *136*, 12892–12895.
- [22] X.-K. Wan, Z.-W. Lin, Q.-M. Wang, *J. Am. Chem. Soc.* **2012**, *134*, 14750–14752.
- [23] B. S. Guttrath, I. M. Oppel, O. Presly, I. Beljakov, V. Meded, W. Wenzel, U. Simon, *Angew. Chem. Int. Ed.* **2013**, *52*, 3529–3532; *Angew. Chem.* **2013**, *125*, 3614–3617.
- [24] J. Chen, Q.-F. Zhang, T. A. Bonaccorso, P. G. Williard, L.-S. Wang, *J. Am. Chem. Soc.* **2014**, *136*, 92–95.
- [25] H. Yang, Y. Wang, J. Yan, X. Chen, X. Zhang, H. Häkkinen, N. Zheng, *J. Am. Chem. Soc.* **2014**, *136*, 7197–7200.
- [26] A. Das, T. Li, G. Li, K. Nobusada, C. Zeng, N. L. Rosi, R. Jin, *Nanoscale* **2014**, *6*, 6458–6462.
- [27] Y. Song, S. Wang, J. Zhang, X. Kang, S. Chen, P. Li, H. Sheng, M. Zhu, *J. Am. Chem. Soc.* **2014**, *136*, 2963–2965.
- [28] C. Zeng, H. Qian, T. Li, G. Li, N. L. Rosi, B. Yoon, R. N. Barnett, R. L. Whetten, U. Landman, R. Jin, *Angew. Chem. Int. Ed.* **2012**, *51*, 13114–13118; *Angew. Chem.* **2012**, *124*, 13291–13295.
- [29] Y. Shichibu, Y. Negishi, T. Watanabe, N. K. Chaki, H. Kawaguchi, T. Tsukuda, *J. Phys. Chem. C* **2007**, *111*, 7845–7847.
- [30] A. Das, T. Li, K. Nobusada, Q. Zeng, N. L. Rosi, R. Jin, *J. Am. Chem. Soc.* **2012**, *134*, 20286–20289.
- [31] H. Yang, Y. Wang, J. Lei, L. Shi, X. Wu, V. Mäkinen, S. Lin, Z. Tang, J. He, H. Häkkinen, L. Zheng, N. Zheng, *J. Am. Chem. Soc.* **2013**, *135*, 9568–9571.
- [32] S. Wang, X. Meng, A. Das, T. Li, Y. Song, T. Cao, X. Zhu, M. Zhu, R. Jin, *Angew. Chem. Int. Ed.* **2014**, *53*, 2376–2380; *Angew. Chem.* **2014**, *126*, 2408–2412.
- [33] D. M. Chevrier, A. Chatt, P. Zhang, C. Zeng, R. Jin, *J. Phys. Chem. Lett.* **2013**, *4*, 3186–3191.
- [34] R. Jin, *Nanoscale* **2015**, *7*, 1549–1565.
- [35] P. Maity, S. Takano, S. Yamazoe, T. Wakabayashi, T. Tsukuda, *J. Am. Chem. Soc.* **2013**, *135*, 9450–9457.
- [36] P. Maity, T. Wakabayashi, N. Ichikuni, H. Tsunoyama, S. Xie, M. Yamauchi, T. Tsukuda, *Chem. Commun.* **2012**, *48*, 6085–6087.
- [37] X.-K. Wan, Q. Tang, S.-F. Yuan, D.-e. Jiang, Q.-M. Wang, *J. Am. Chem. Soc.* **2015**, *137*, 652–655.
- [38] H. Qian, Y. Zhu, R. Jin, *ACS Nano* **2009**, *3*, 3795–3803.
- [39] H. Yang, Y. Wang, A. J. Edwards, J. Yana, N. Zheng, *Chem. Commun.* **2014**, *50*, 14325–14327.
- [40] D. Crasto, S. Malola, G. Brosofsky, A. Dass, H. Häkkinen, *J. Am. Chem. Soc.* **2014**, *136*, 5000–5005.
- [41] H. Qian, W. T. Eckenhoff, Y. Zhu, T. Pintauer, R. Jin, *J. Am. Chem. Soc.* **2010**, *132*, 8280–8281.
- [42] G. Li, D.-E. Jiang, C. Liu, C. Yu, R. Jin, *J. Catal.* **2013**, *306*, 177–183.
- [43] P. J. Krommenhoek, J. Wang, N. Hentz, A. C. Johnston-Peck, K. A. Kozek, G. Kalyuzhny, J. B. Tracy, *ACS Nano* **2012**, *6*, 4903–4911.
- [44] C. Zeng, Y. Chen, K. Kirschbaum, K. Appavoo, M. Y. Sfeir, R. Jin, *Sci. Adv.* **2015**, *1*, e1500045.
- [45] C. Zeng, Y. Chen, G. Li, R. Jin, *Chem. Mater.* **2014**, *26*, 2635–2641.
- [46] J.-i. Nishigaki, R. Tsunoyama, H. Tsunoyama, N. Ichikuni, S. Yamazoe, Y. Negishi, M. Ito, T. Matsuo, K. Tamao, T. Tsukuda, *J. Am. Chem. Soc.* **2012**, *134*, 14295–14297.

Received: March 25, 2015

Published online: July 1, 2015